STScI | SPACE TELESCOPE SCIENCE INSTITUTE

Instrument Science Report WFC3 2022-01

Cold and Unstable Pixels in WFC3/IR

Harish Khandrika

March 15, 2022

Abstract

We examined the pixel stability and "heat" in the Cycle 28 IR dark files which are used to create the latest IR bad pixel table. Between November 2020 and November 2021 the number of cold and unstable pixels increased by 1.7%, compared to only 0.5% the previous cycle. 91% of cold and unstable pixels were flagged as random telegraph noise and highly variable. The overall median dark current has increased by 6.5% while the error has decreased by 2% in Cycle 28 leading to the increased number of cold and unstable pixels. Trends in dark counts and error levels were checked against a number of telemetry trends but no correlations were found. It is possible that low-level or undetectable changes in detector temperature or voltage could produce the observed 0.08 counts/sec change. We determined that these trends began before the July 14 2021 side-switch of some of the SI C&DH memory modules and electronics and are therefore unrelated to that event. We examined additional potential detector issues and searched for matching and correlating trends but none were found.

1 Introduction

The WFC3/IR detector has an innate thermal background that is present in all images. This background, called a dark current, can be viewed when the instrument is "exposed" with an aluminum blank in the light path. Periodically, the dark current is measured and dark files are generated that are used for correction of the thermal background as well as for examining the quality of the IR detector pixels. Regions of the detector that negatively impact science quality are considered bad pixels, and a reference file - the IR bad pixel table (hereafter IR BPIXTAB) - is created to help observers avoid the use of these pixels for

science (Hilbert 2012). As part of the bad pixel table creation, we measure the heat and the stability of bad pixels in order to better characterize the weathering of the IR detector over time (Sunnquist, Brammer, and Baggett 2019). A pixel is considered "hot" if it maintains or reaches a particular count-rate level that is well outside the nominal thermal background levels. A pixel can be considered unstable for various reasons such as random telegraph noise or high variability. We report here on the trends in heat and stability seen in the Cycle 28 (November 2020 - Oct 2021) IR BPIXTAB.

2 Data

Data were obtained through the MAST Hubble Archive and consisted of 24 full-frame WFC3/IR images from the Cycle 28 (Nov 2020 - Oct 2021) dark monitor calibration program 16403. This data set was used along with the Cycle 28 internal flat-fields monitor program 16411 data for the creation of the Cycle 28 IR bad pixel table. The darks are observed using the SPARS200 mode and NSAMP16 (16 sample ramps) with a total exposure time of 2800s, and are used for the flagging of unstable and hot pixels. The darks are observed twice a month for 12 months in the cycle resulting in 24-26 dark files for the entire cycle. The full methodology for creation of the bad pixel table and for the time-dependent analysis can be found in (Sunnquist 2019).

3 Analysis

3.1 Stability and heat

Figure 1 shows the percentage of the WFC3/IR detector that is composed of cold, hot, stable, and unstable pixels over time. The percentages for each layer is cumulative, totaling 100% of the detector pixels. The hot and unstable pixel layer (red) increased by 0.20% and the cold and unstable pixels (blue) increased by 1.73% (to 2.85%) between 2020 and 2021 (Cycle 27 to Cycle 28). While 2.85% of the detector pixels is a relatively small percentage, the sudden jump in the last cycle was a more significant increase than seen in previous cycle transitions, warranting further inspection and analysis.

Figure 2 shows the positions of the new cold and unstable pixels in Cycle 28. While some appear in the "death star" region (Hilbert and McCullough 2009), the vast majority of pixels are found dispersed randomly and uniformly throughout the detector frame, indicating that neither persistence nor other isolated points were the sole reason for the increase. Though 2 shows an increase of 1.92% this is only counting the newly formed cold and unstable pixels in Cycle 28, and does not account for any unstable pixels from Cycle 27 that became stable in Cycle 28. Factoring those pixels results in the 1.73% increase as previously mentioned.

To check the uniformity we compared the new Cycle 28 cold and unstable pixels with a randomly generated uniform 2D noise image with 1.92% of pixels flagged throughout the image. The comparison was performed using the Kolmogorov–Smirnov (KS) test (Karson 1968) which provides the probability that the observed sample could be drawn from a given

model probability distribution. SciPy's [1] KS test module provides the KS statistic as well as a p-value for null-hypothesis testing. The KS statistic, in essence, is the largest absolute difference between the two input functions, and a result of 0 indicates that the sample comes from the model distribution.

For the points in Figure 2, the KS-statistic reported was 4.67×10^{-4} with a p-value of 0.9998, indicating that these unstable pixels are randomly and uniformly distributed throughout the detector. Confidence checks for the KS test were performed by cutting out pixels comprising the "death star", setting all pixels to 0 or 1, and testing more patterned (i.e. non-uniform) images for which all of the KS tests resulted in high KS-statistic values or low p-values, or both.

3.2 Dark current rate between cycles

Figure 3 shows the dark current rate for the individual constituent darks used to create the Cycle 27 BPIXTAB. While there appears to be a slight decrease in overall dark current levels, it is within the intrinsic scatter and the linear fit's r^2 value of 0.02 shows that the coefficient of determination is low. For comparison, Figure 4, shows the dark current rate for the constituent darks used to create the Cycle 28 BPIXTAB. The dark current rate seems to decrease from 0.026 to 0.018 counts per second ($\sim$44.4% decrease), and the linear fit r^2 (0.389) shows a stronger coefficient of determination. We investigated whether these trends were seen in past dark current images used for previous cycle IR BPIXTABs and the results are shown in Figure 5. Overall trends in the dark current levels seem to be moderate or steady for the past 8 years and significant drops are only seen in 2009, 2010, 2013, and 2021. The Cycle 29 dark current level has remained within the intrinsic scatter of the data with no large deviations. Declining trends in past cycles have not corresponded with any increases in cold and unstable pixels, and so we do not attribute the declining dark current rates in Cycle 28 to this new increase.

3.3 Could the changes be due to the July 2021 side switch?

In mid-June 2021, a memory module issue occurred on the NASA Standard Spacecraft Computer-1 (NSSC-1), causing a lockup and safing of the science instruments[2]. Various tests were performed of the memory modules on side B of the Calibration Unit / Science Data Formatter (CU/SDF) in the Science Instrument Command Data Handling (SI C&DH). Memory module handshake failures occurred with the CU/SDF side B and so, on July 14 2021, flight software updates were pushed to the telescope to switch to the side A CU/SDF of the NSSC-1.

This shift in memory modules and sides is not thought to have any effect on the performance of the science instruments. However, given that it was the single largest deviation in routine between cycles, we flagged the the side switch as the initial candidate when we began investigating the increase in the cold and unstable pixels. Figures 4 and 5 have the time of the side-switch flight software push indicated with a blue vertical line. Post-side-switch dark

[1] https://docs.scipy.org/doc/scipy/reference/generated/scipy.stats.ks_2samp.html

[2] https://www.stsci.edu/contents/newsletters/2021-volume-38-issue-02/hst-stsci-update

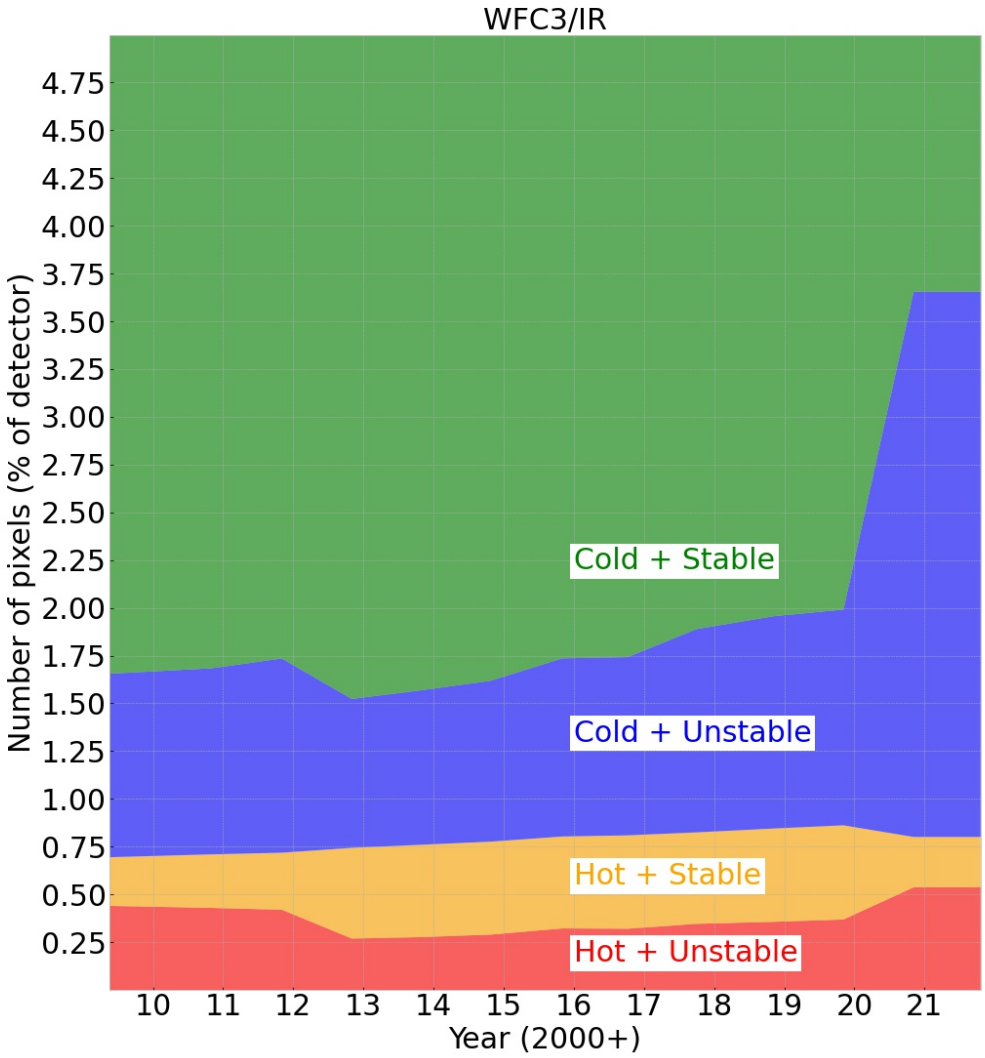

Figure 1: Pixel stability chart over time for WFC3/IR, including the latest Cycle 28 data. Each layer in the chart is stacked, so absolute percentages are aggregated and total to 100%. Note that the y-axis caps at 5%, meaning that over 95% of pixels are cold and stable (i.e. good).

current levels, while lower than the cycle start, were within the levels seen just before the side-switch occurred. The BPIXTAB was generated again, excluding the post-side-switch dark current and flat-field files, in order to further test if the side-switch was the main cause of the instability. Similarly a post-side-switch-only BPIXTAB was also generated to measure these levels. The percentage of cold and unstable pixels rose by a factor of 2 when side-switch data are excluded, while the percentage rose by a factor of 4 when only the side-switch data

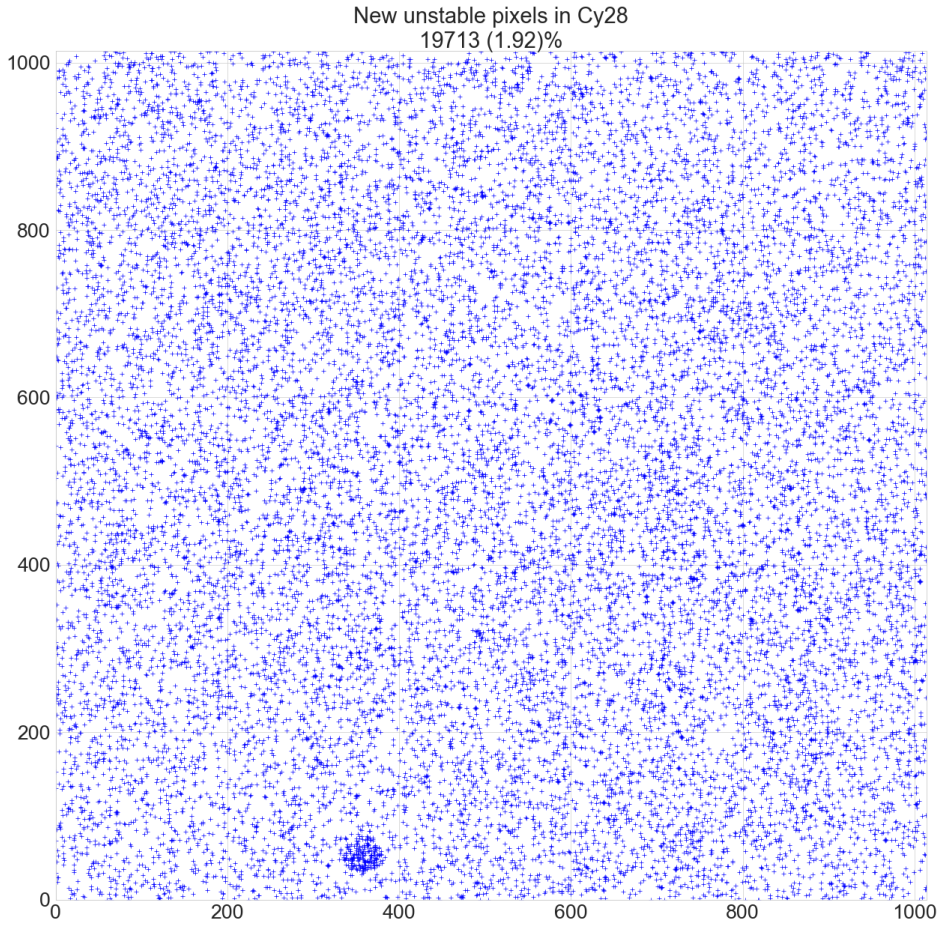

Figure 2: The positions of new cold and unstable pixels that appeared **for the first time** in Cycle 28. The number of pixels and the equivalent percentage are shown in the figure title. The pixels are distributed uniformly across the detector, except for an enhancement in the "death star" region (round feature centered at X,Y of 380, 50).

were used. We attribute both of these increases to the lack of sufficient data and we do not attribute any IR BPIXTAB changes to the side-switch.

3.4 Testing conditions for cold and unstable pixels

The IR BPIXTAB creation program tests the individual darks across the cycle for various conditions in order to be marked as unstable (Sunnquist, Brammer, and Baggett 2019). In order to determine if there was a singular cause for the majority of the flagging of unstable pixels, the data were examined for each condition individually.

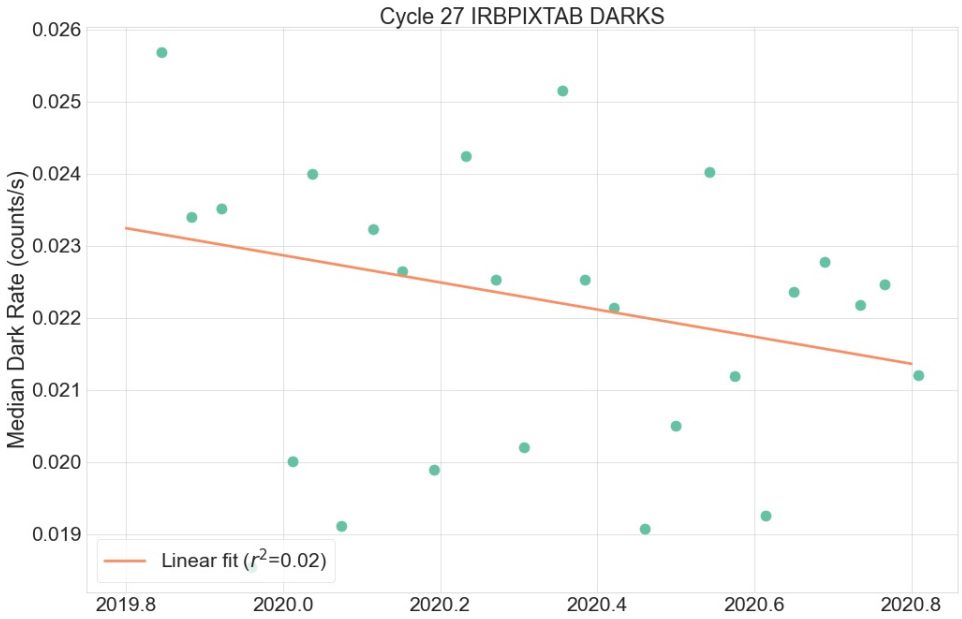

Figure 3: Median dark current rate for all the constituent dark current files that were used to create the Cycle 27 (Nov 2019-Oct 2020) IR bad pixel table. A linear fit is overplotted with the corresponding r^2 coefficient of determination measurement.

3.4.A Varying more than 3 times expected error

Across all darks through the cycle used in creation of the BPIXTAB, the median absolute deviation (MAD) is computed and is compared to the median error taken from the ERR array for each dark. If this ratio between the MAD and error is greater than three (effectively above 3-sigma), this pixel is classified as unstable. Figure 6 shows the position of all pixels that match this condition, amounting to ∼40% of all new cold and unstable pixels in Cycle 28. Figure 7 shows a random sample of 10 pixels that match this condition compared to 10 normal cold and stable pixels.

3.4.B Very high observed variability

The second condition simply tests pixels for extremely high variability. A pixel whose standard deviation across the time-axis is greater than 0.05 is flagged as unstable. Figure 8 shows the position of all pixels that match this condition, amounting to approximately 15% of all new cold and unstable pixels. Note that this percentage may include pixels that also match condition A and other conditions. Figure 9 shows a random sample of 10 pixels that match this condition compared to 10 normal cold and stable pixels.

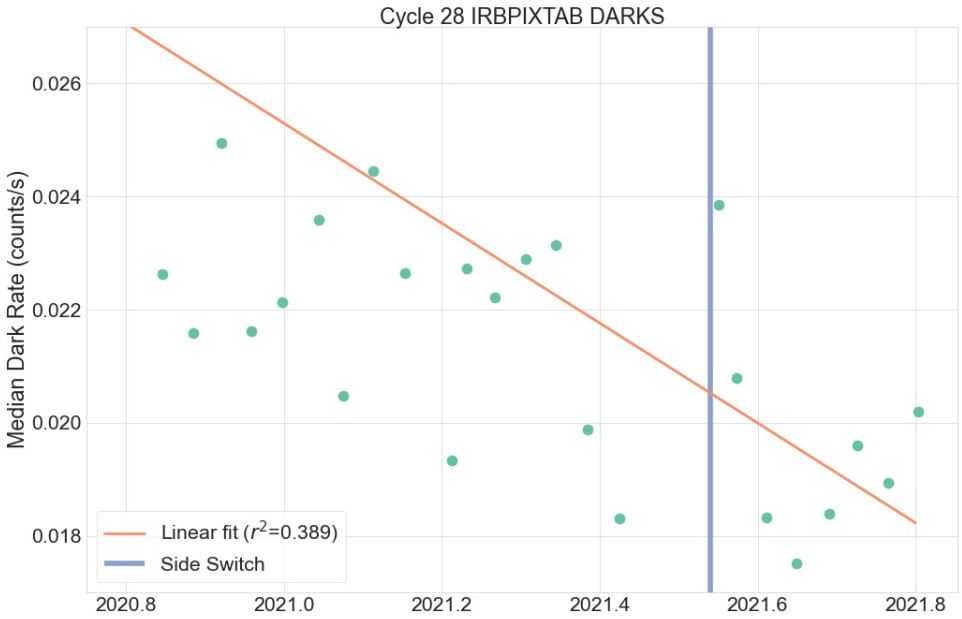

Figure 4: Similar to Figure 3 but for the Cycle 28 IR bad pixel table (Nov 2020 - Oct 2021). The blue vertical line denotes the time of the 2021 HST side-switch.

3.4.C High variation in earliest or latest observations

The third condition looks for pixels that show high variation either earlier in the cycle or later in the cycle. This test divides the usual 24 dark current files for a cycle's IR BPIXTAB into 3 groups and tests the first 8 files and (separately) the last 8 files for pixels that are 4 times the median absolute deviation level (synonymous with 4-sigma). Figure 10 shows both the early MAD and late MAD variability pixels, however only 2%-3% match condition C.

3.4.D Pixels that jump between very different signal levels throughout the cycle

The fourth condition does an important test that looks for any pixels that jump between very different signal levels throughout the observations. This condition is tested by again splitting the dark current files into 3 groups of 8 representing the beginning, middle and end of the cycle. Each group's median dark current level is taken (across the time axis) and then compared to each other. That is, differences between early-to-late, early-to-middle, and middle-to-late compared to the expected error. If any of these differences are greater than 4 times the expected error (4-sigma), these pixels are flagged as unstable. Figure 11 shows the position of all pixels that match this condition. Approximately 91% of all cold-and-unstable pixels this cycle match this particular condition, though overlap with other conditions reduces this to approximately 50% purely matching this condition only. Figure 12 shows the random sample as before for 10 pixels that match this condition compared to

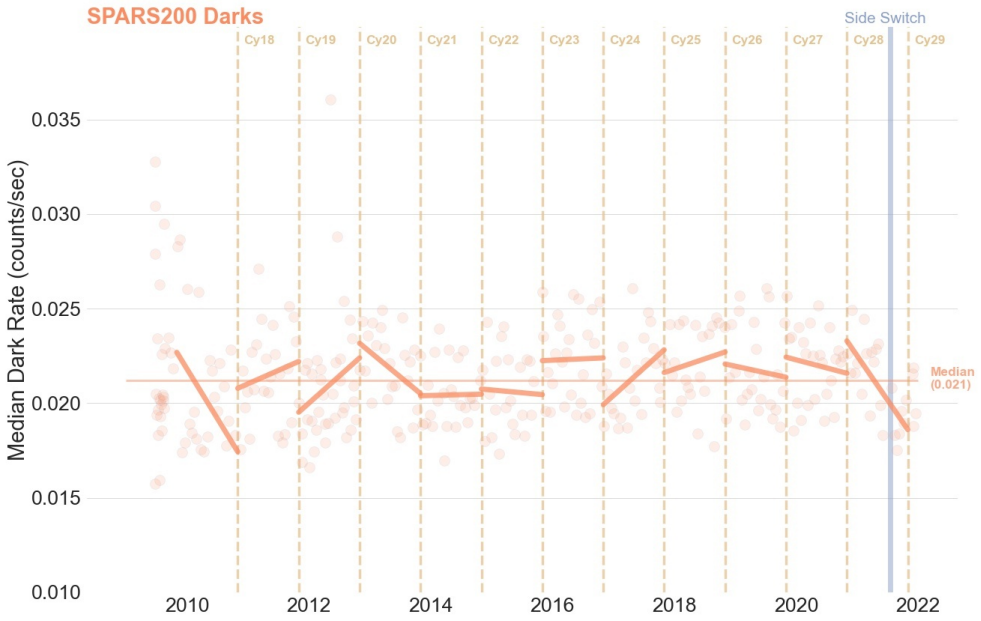

Figure 5: Every SPARS 200 dark current image used in the creation of the IR bad pixel tables for each cycle. The cycle boundaries are marked by the vertical dashed line, and slopes were fitted to the data for each cycle from 2010 onwards. The 2009 data were not fit. The Mid-2021 HST side switch is marked with a vertical blue line.

normal pixels.

3.4.E Random Telegraph noise

The penultiumate condition tests for random telegraph noise which is present in semiconductors and detectors and manifests as sudden shifts in discrete voltage levels. This may occur in detectors via trapping and subsequent release of stored charges due to defects in the oxide or interfaces. The condition is met ia a pixel varies by more than 6-sigma throughout the cycle. Figure 13 shows the position of these pixels which comprise 70% of the new cold and unstable pixels (with potential overlap with other conditions). Figure 14 shows the random sample of telegraph noise pixels compared to the same 10 random cold and stable pixels.

3.4.F Zero or infinite ratio pixels

This final condition simply looks for any pixels that have zero or infinite MAD-to-error ratios and possibly occur due to up-the-ramp instability or saturation. Only one pixel was found to match this condition.

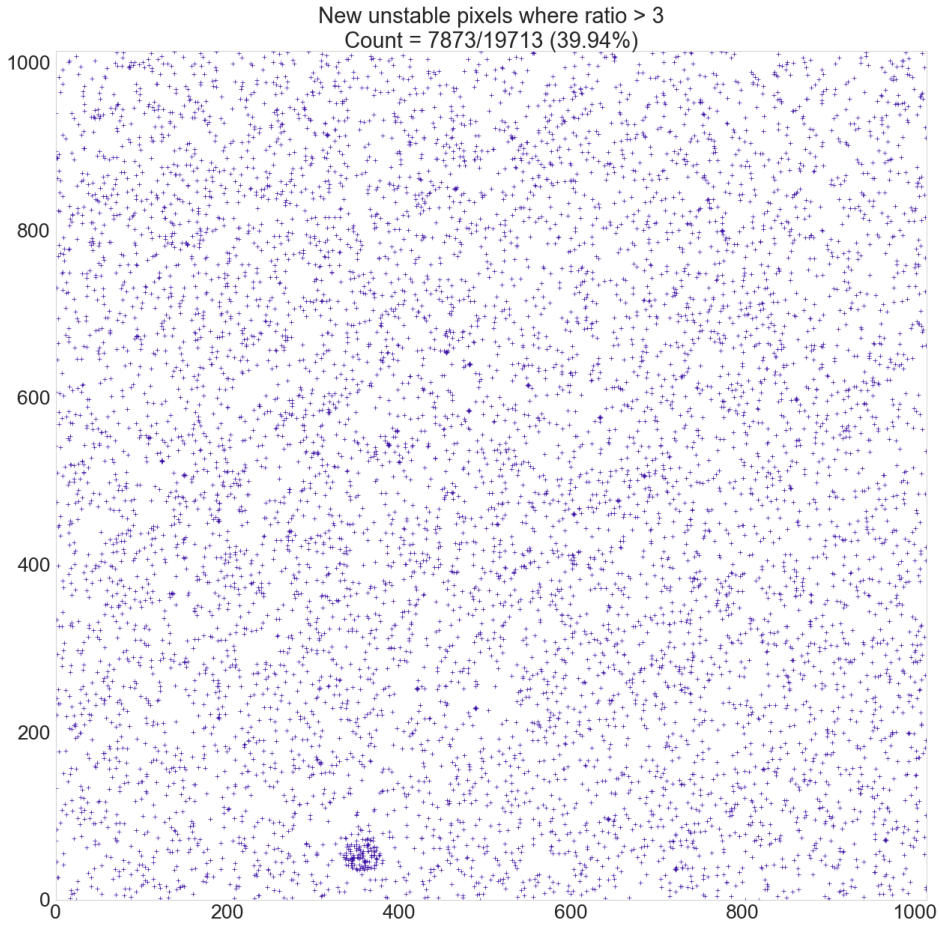

Figure 6: All cold and unstable pixels that match condition A (varying more than 3 times the expected error). The percentage and number of pixels in the figure title represent the total number of new cold and unstable pixels that appeared in Cycle 28 only.

3.5 Median absolute deviation and error over time

Conditions A, C and D rely upon the ratio of the median absolute deviation to the median error in the darks across the entire cycle time period. About 91% of new cold and unstable pixels for Cycle 28 have shown to match condition D in particular, and so examination of the MAD and error over time is imperative. Figures 15 and 16 show the MAD and error over time for Cycles 27 and 28 with linear fits and the side-switch marked. The MAD and median error were computed over the entire dark current image frame for each point in time. The MAD for Cycle 28 has increased with time, with a significant excursion 2 months after the side-switch, while the average error (from the ERR array in each dark current) has fallen, dropping significantly after the side-switch. Distributions of the error array for each dark

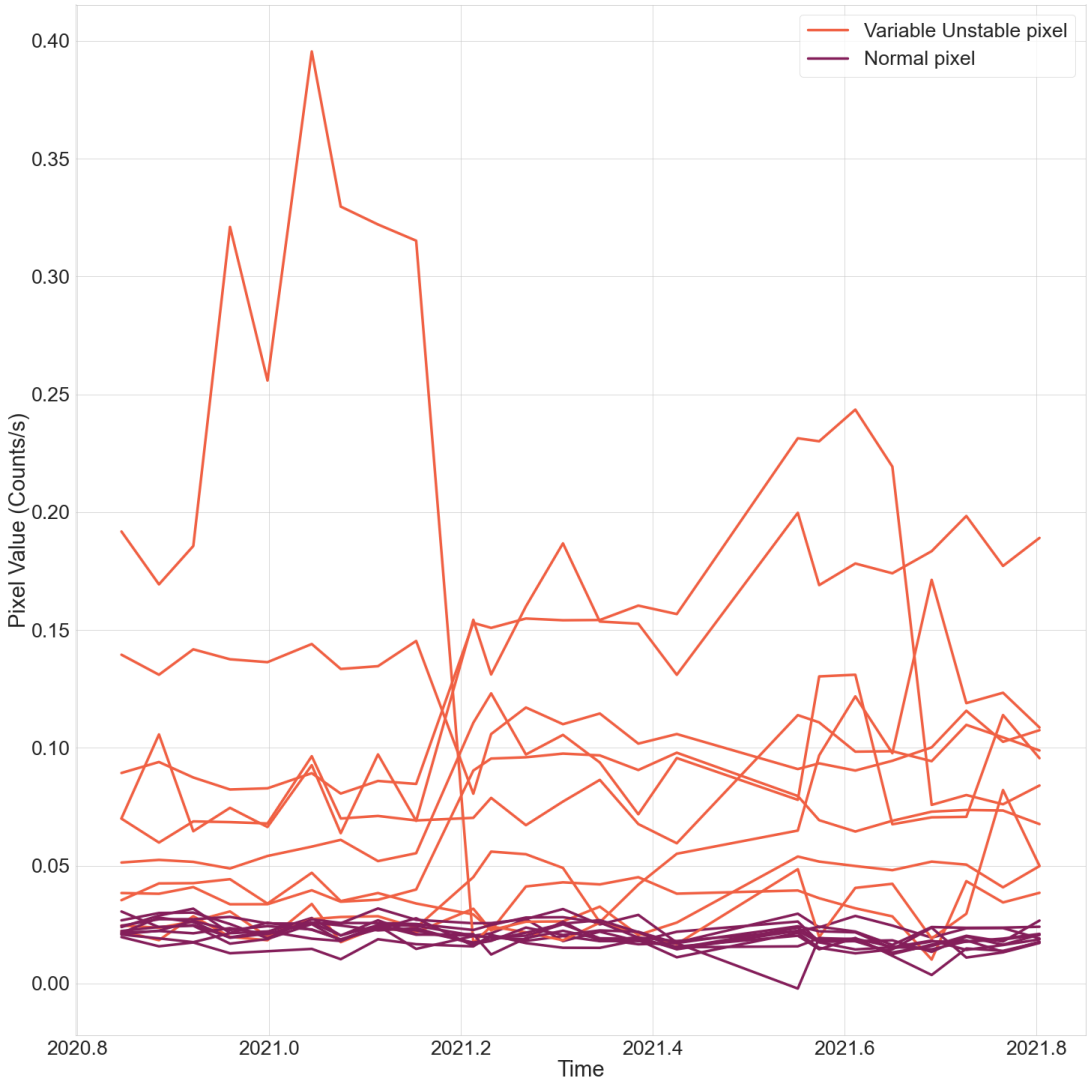

Figure 7: A sample of 10 random pixels that match condition A which vary more than 3 times the expected error compared to 10 random normal cold and stable pixels. The pixel value in counts/second is shown in the y-axis and the dates for each dark current image in Cycle 28 are shown on the x-axis.

current image used in the cycle's BPIXTAB are shown in the ridge plot in Figure 17 with the earliest dark current on top and the latest toward the bottom. The distributions reflect the results seen in Figure 16, namely that the error has been decreasing over time.

4 Discussion

Based on our analysis, it is clear that the rise in cold and unstable pixels through 2021 was due to highly temporally variable pixels and telegraph noise (conditions D and E respectively.) What is unclear is the cause of this increase. Initial speculation was placed on the Mid-2021

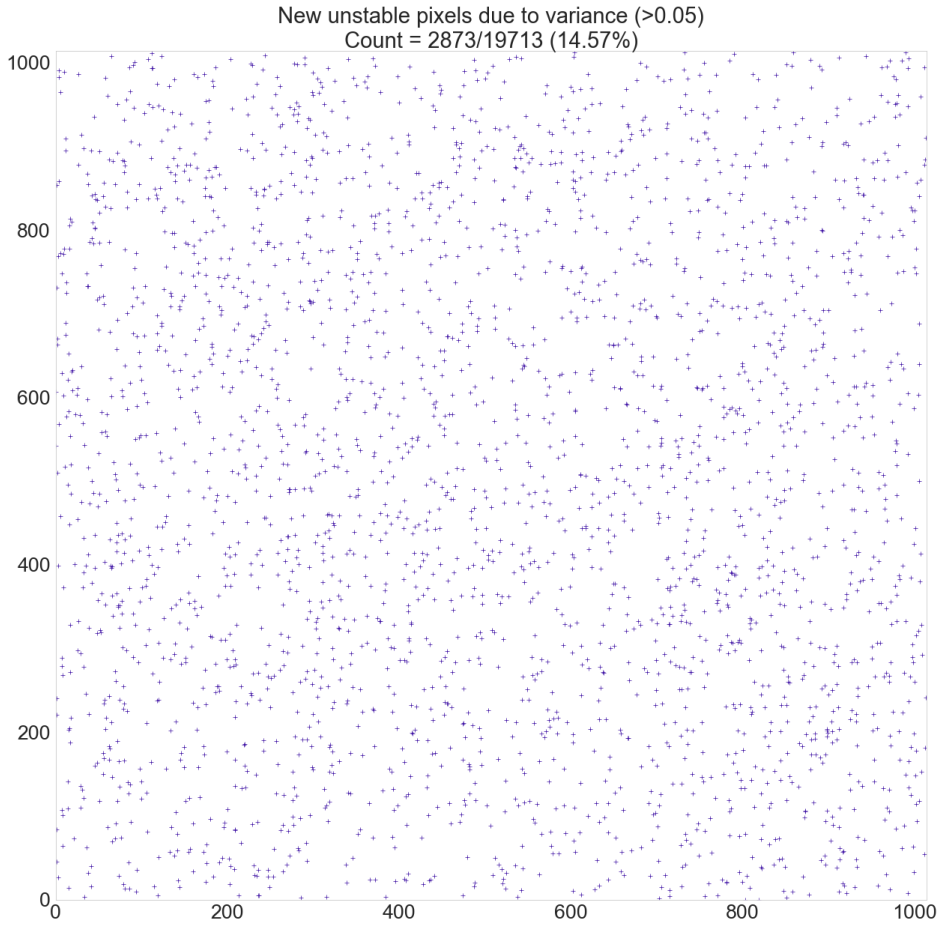

Figure 8: All cold and unstable pixels that match condition B (standard deviation > 0.05). The percentage and number of pixels in the figure title represent the total number of new cold and unstable pixels that appeared in Cycle 28 only.

HST SI C&DH side-switch. Figures 15 and 16 show that post-side-switch MAD and error levels shifted compared to the pre-side-switch levels with some excursions occurring after the switch. However the random sample of pixels seen in Figure 12 and Figure 14 show no such temporal dependence, with excursions occurring at either end of the cycle. Further, no drastic cutoff in the error levels in Figure 17 during the side-switch seens to indicate that the switch was not the cause for the increase.

We examined telemetry data (e.g. temperature, voltage, amperage) obtained through the time-frame of cycles 27 and 28. No overt trends or appropriate shifts were seen, though we do note that the effects may be too small to see. Telegraph noise in particular could manifest at microvolt levels, which may be difficult to discern in the scale of the telemetry

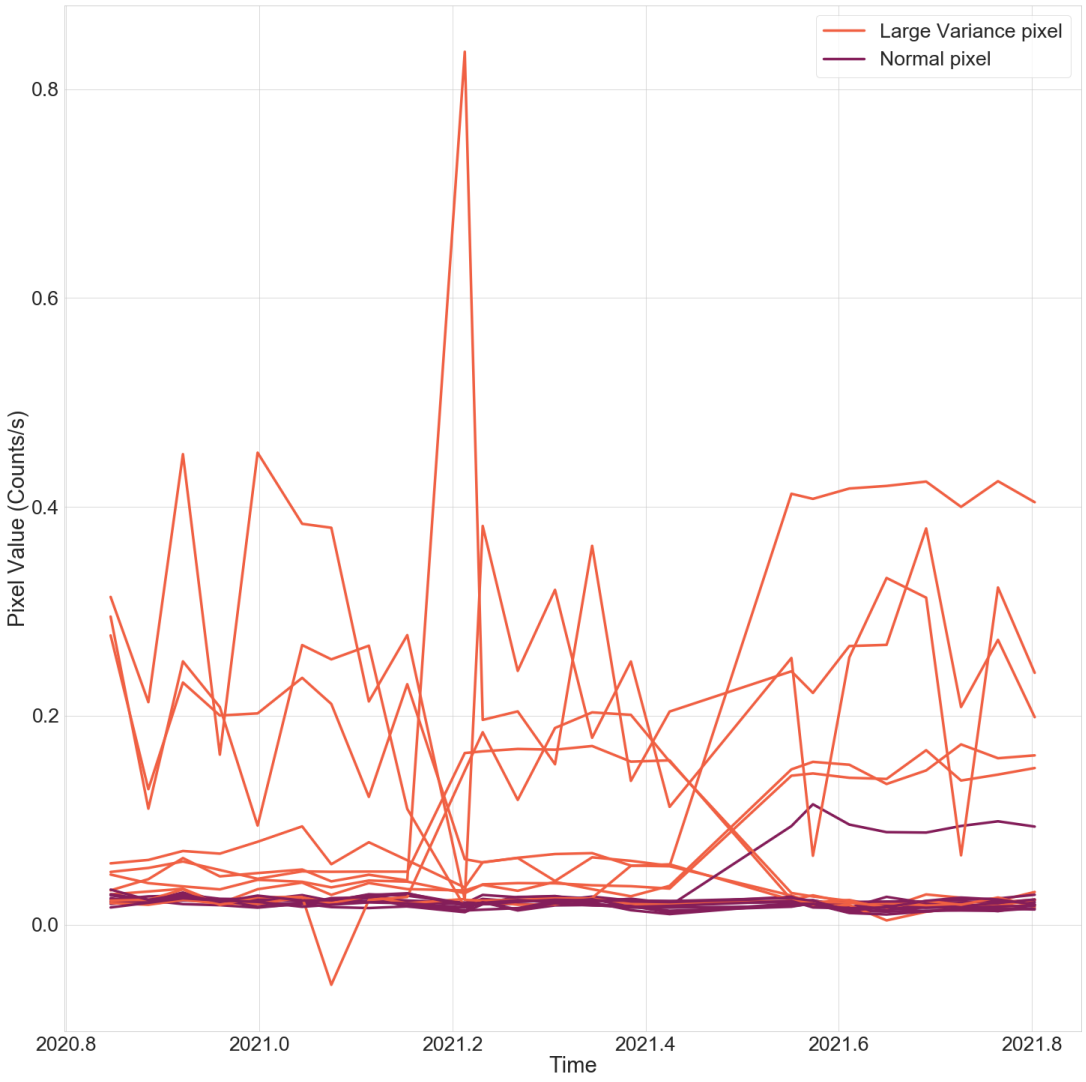

Figure 9: A sample of 10 random pixels that match condition B (standard deviation > 0.05) compared to 10 random normal cold and stable pixels. The pixel value in counts/second is shown in the y-axis and the dates for each dark current image in Cycle 28 are shown on the x-axis.

profiles. Persistence was thought to be a secondary concern as some persistence remained in the constituent dark images. However, we note that the median absolute deviation (MAD) is robust enough to nullify the effects of persistence especially when compared to the standard deviation (which resulted in large swaths of the detector being flagged as unstable or bad in general).

Thus we are unsure of the cause of the increase. We note that the increase is only 1.7% of the detector overall, so the vast majority of pixels (98.3%) are still cold, and stable. We plan to continue tracking these trends through cycles 29 and beyond.

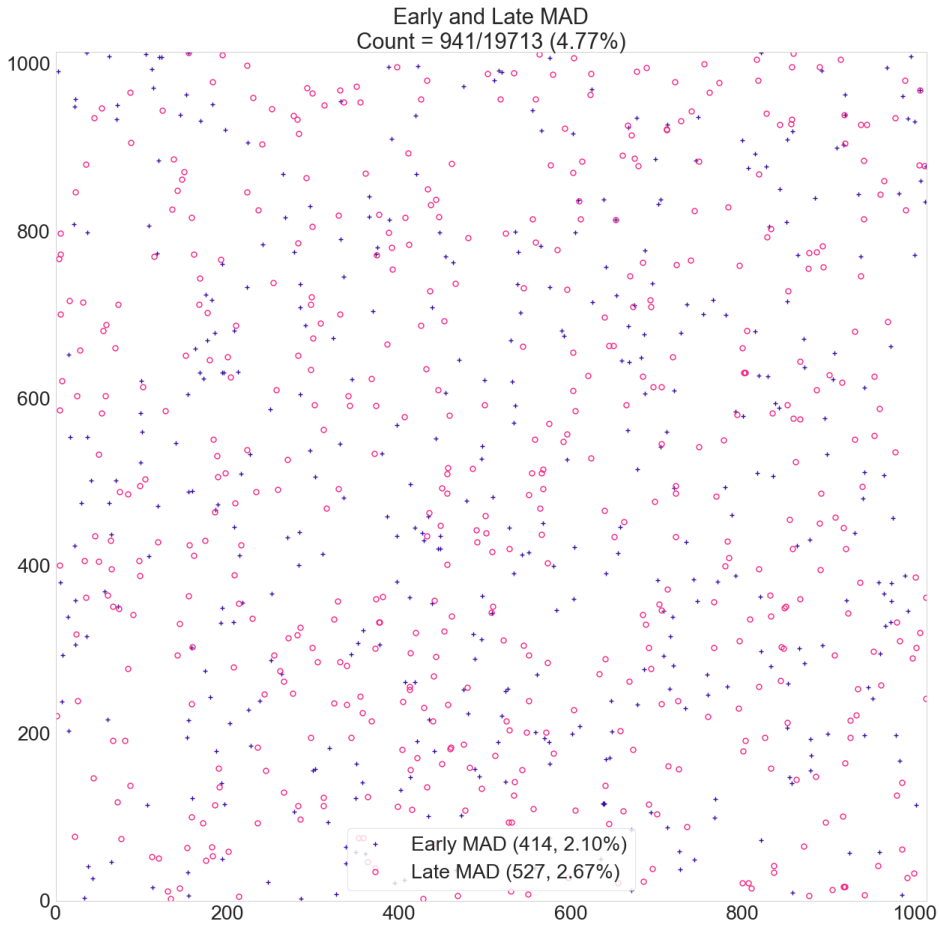

Figure 10: All cold and unstable pixels that match condition C (pixels that vary early or late in the cycle). The plus symbols show all pixels that match this condition in the early part of the cycle, while the circles show all pixels for the late part of the cycle.

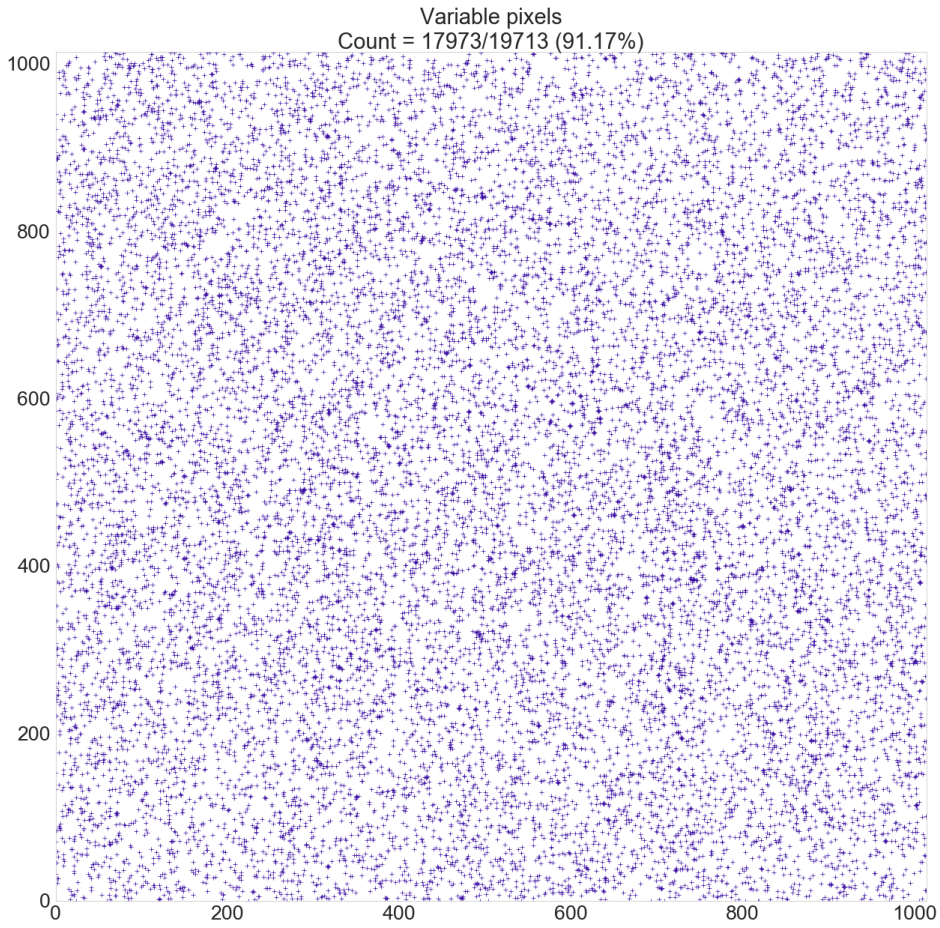

Figure 11: All cold and unstable pixels that match condition D (pixels that jump between very different signal levels throughout the observations). The percentage of pixels given in the title represent all that match this condition but is independent of the other conditions..

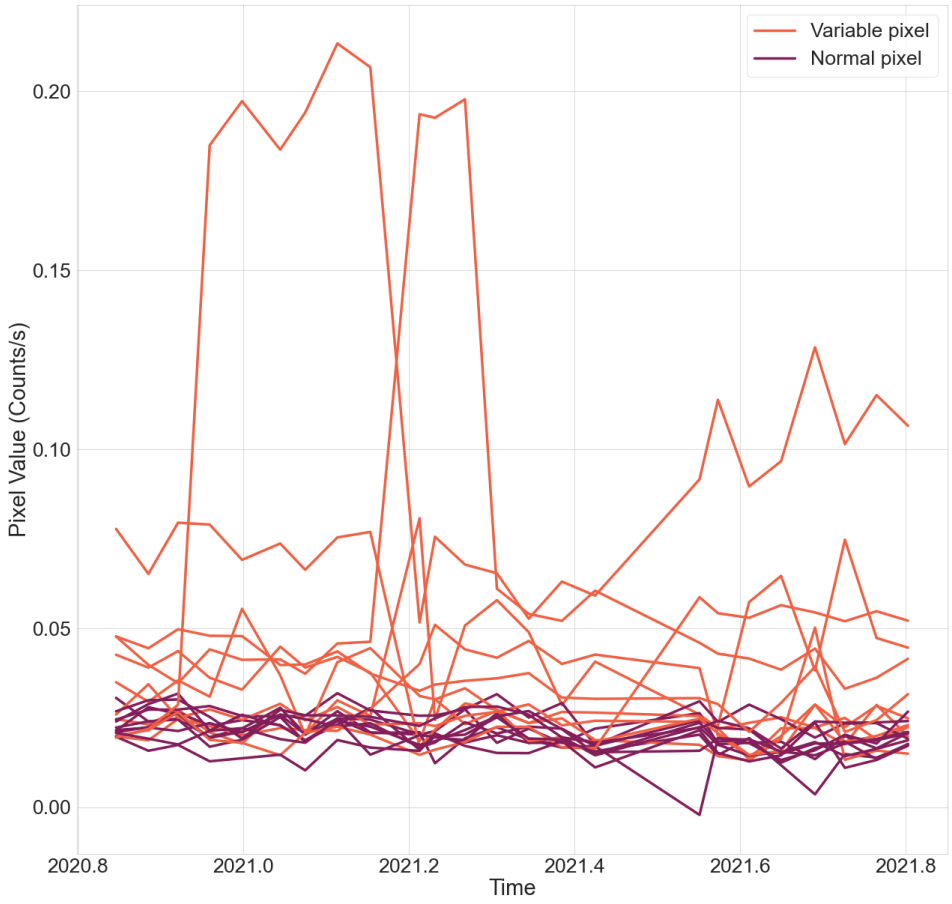

Figure 12: A sample of 10 random pixels that match condition D that jump between very different signal levels throughout the observations. The pixel value in counts/second is shown in the y-axis and the dates for each dark current image in Cycle 28 are shown on the x-axis.

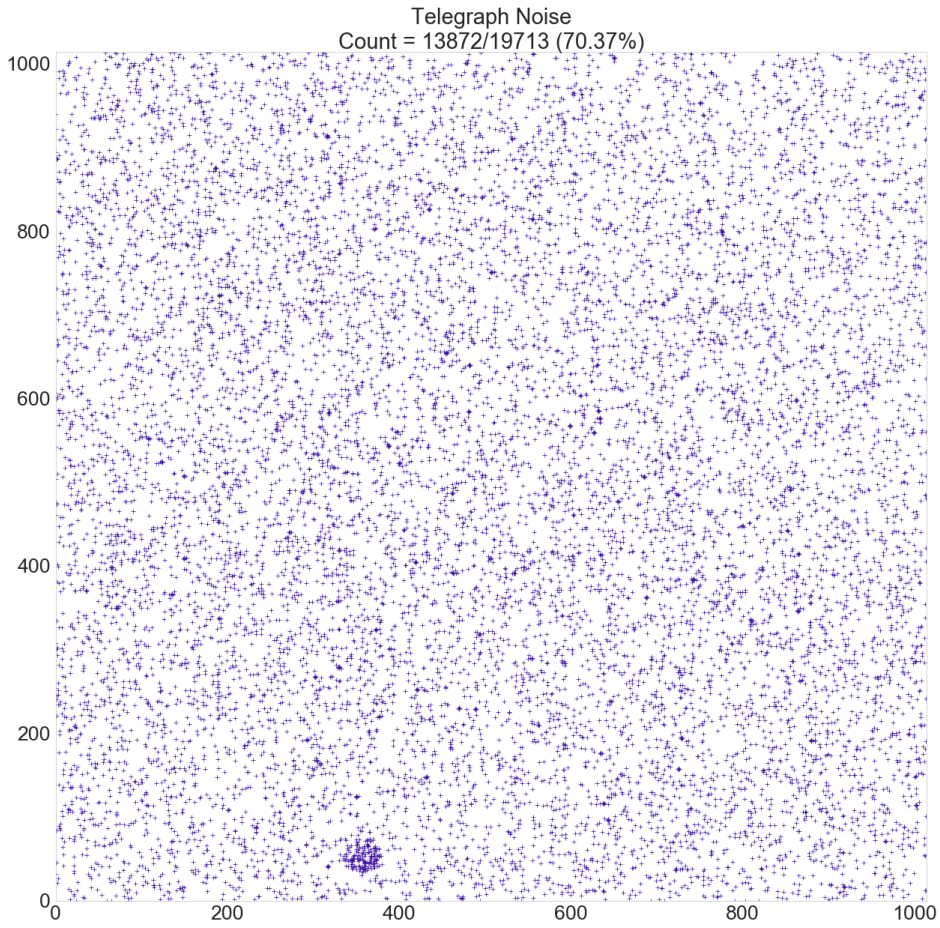

Figure 13: All cold and unstable pixels that match condition E (telegraph noise). The percentage of pixels given in the title represent all that match this condition but there may be overlaps as these pixels match other conditions as well.

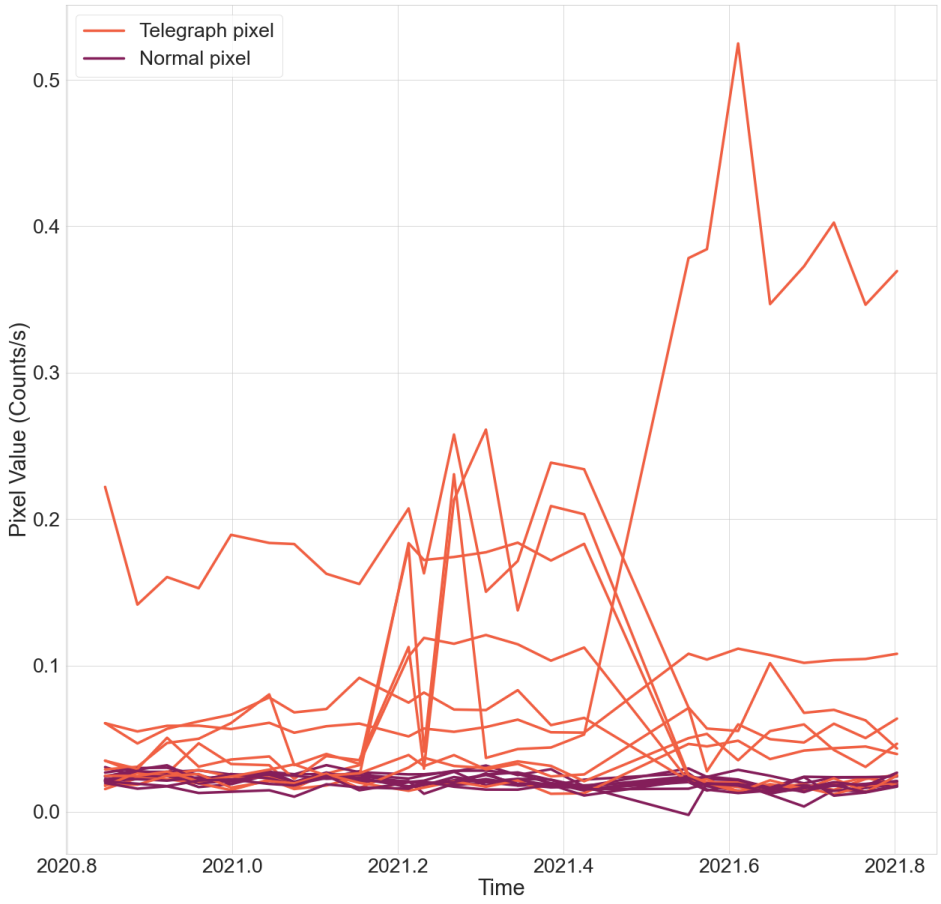

Figure 14: A sample of 10 random pixels that match condition E (telegraph noise). The pixel value in counts/second is shown in the y-axis and the dates for each dark current image in Cycle 28 are shown on the x-axis.

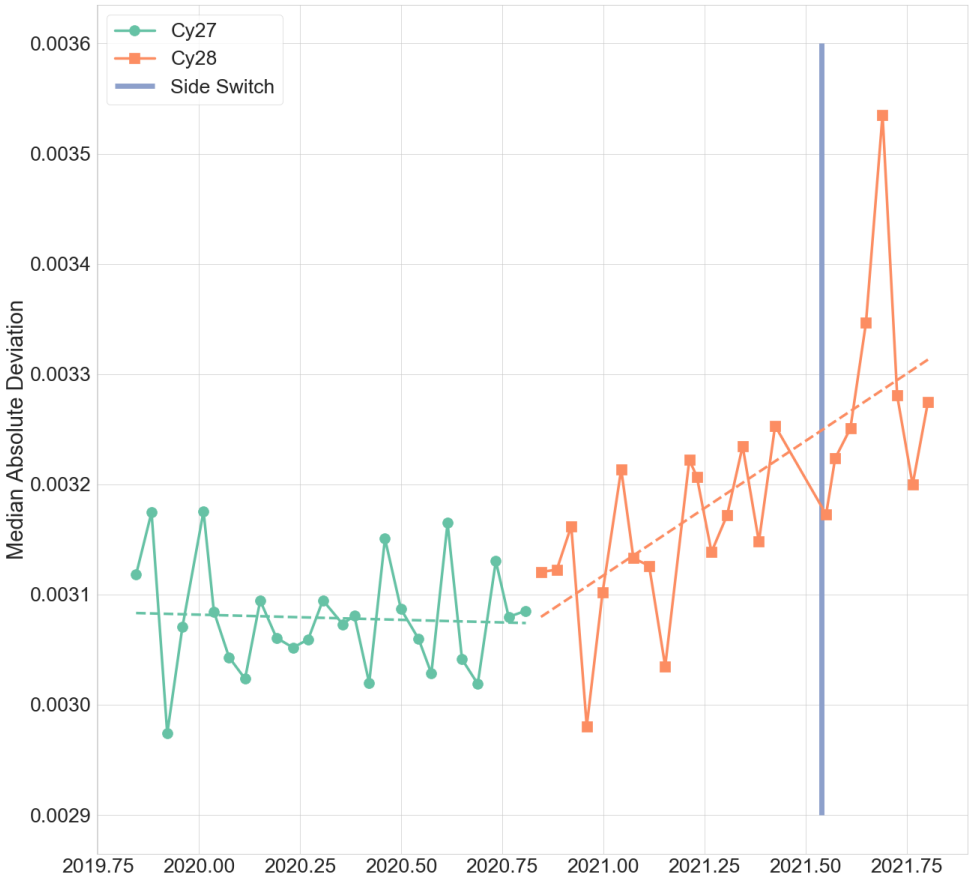

Figure 15: The MAD over time for cycles 27 (green circles) and 28 (orange squares) with linear fits overplotted. The blue vertical line represents the mid-2021 HST SI C&DH side-switch.

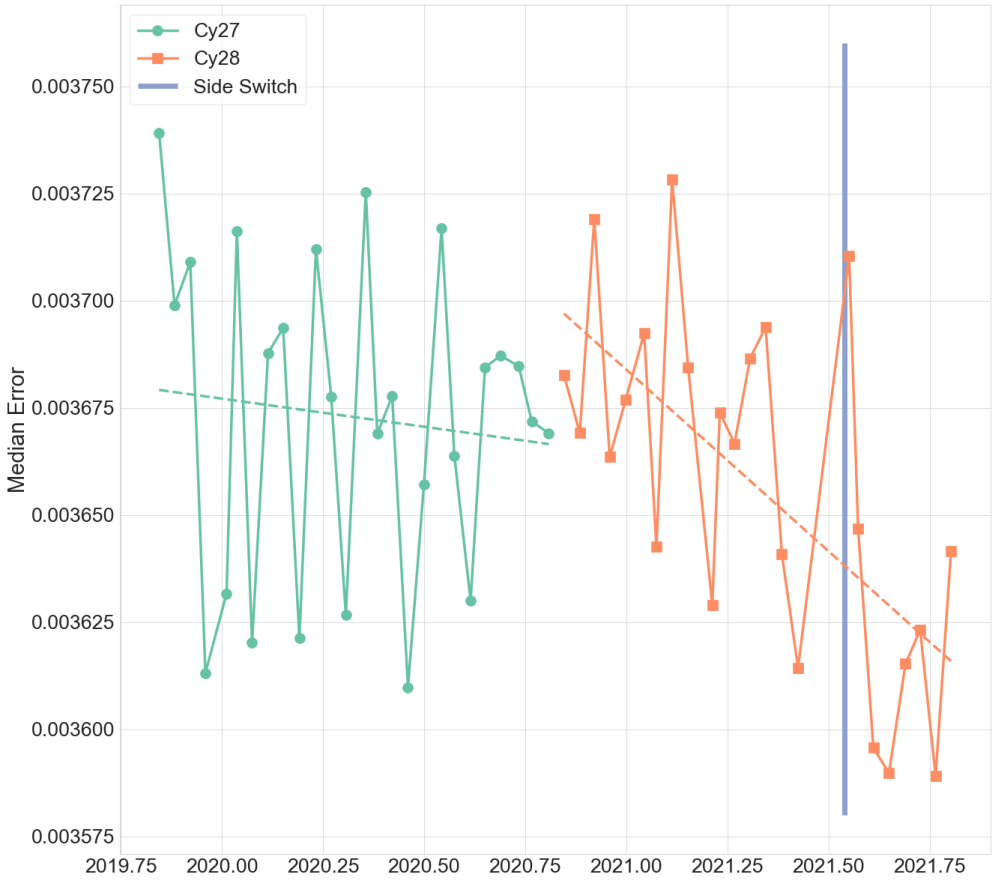

Figure 16: The median error over time for cycles 27 (green circles) and 28 (orange squares) with linear fits overplotted. The blue vertical line represents the mid-2021 HST SI C&DH side-switch.

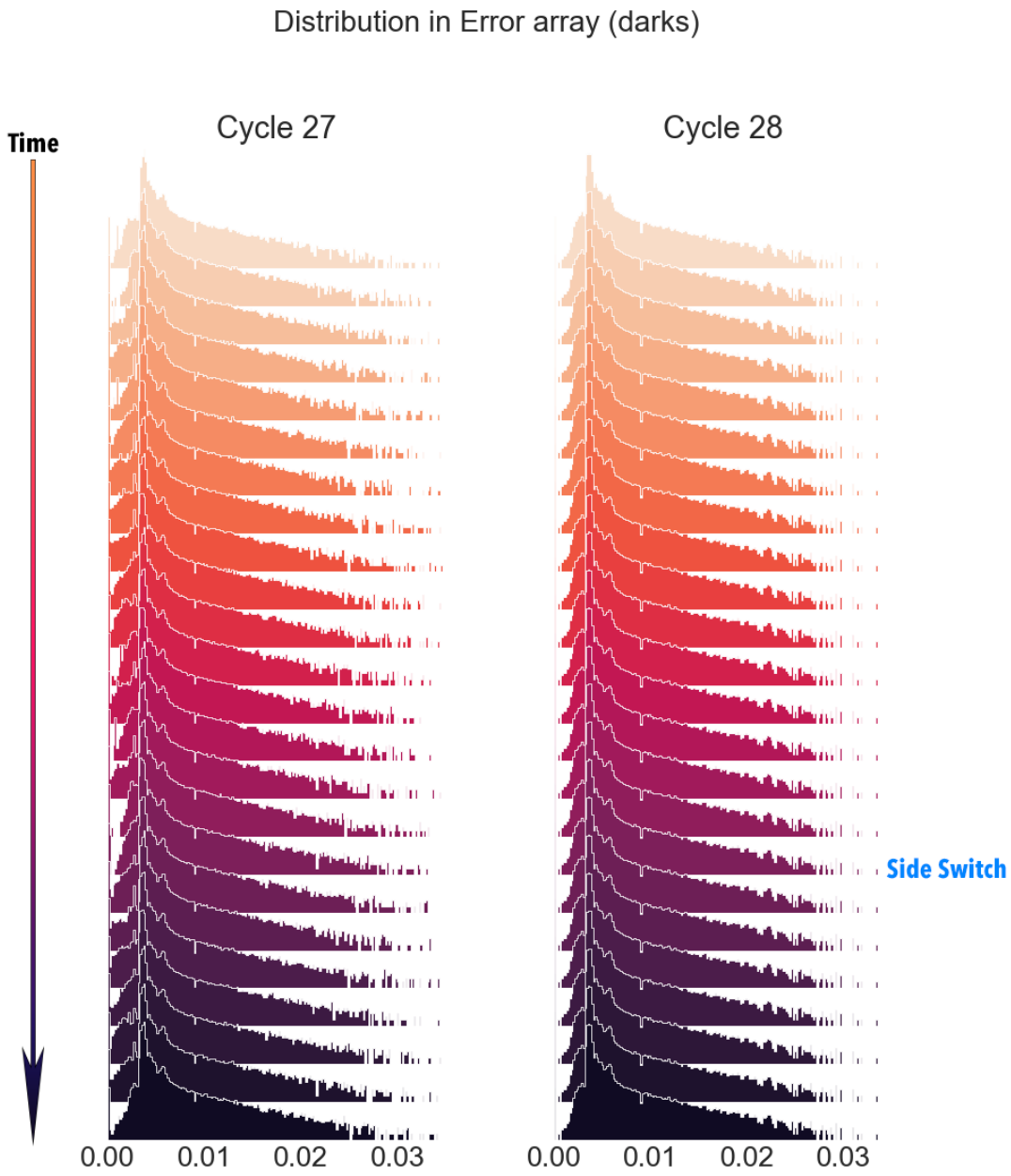

Figure 17: Ridge plot showing histograms/distributions of the error of each dark current frame used in cycles 27 (left) and Cycle 28 (right). The earliest dark current in the cycle is at top (in orange) and descends with the latest at the bottom in black.

5 Conclusions

We examined the pixel stability as computed by the generation of the Cycle 28 WFC3/IR bad pixel table. Between November 2020 and November 2021 the number of cold and unstable pixels increased by 1.7%, compared to only 0.5% the previous cycle. 91% of the cold and unstable pixels were flagged as random telegraph noise and highly variable. The overall median dark current has increased by 6.5% while the error has decreased by 2% in Cycle 28 leading to the increased number of cold and unstable pixels. Trends in dark counts and error levels were checked against various telemetry data such as voltage, temperature, and current but no connections were made. We determined that these trends began before the July 14 2021 side-switch of some of the SI C&DH memory modules and electronics and are therefore unrelated to that event. We examined additional potential detector issues and searched for matching and correlating trends but none were found.

6 Acknowledgments

The author would like to thank Sylvia Baggett, Peter McCullough, Mireia Montes, and Jennifer Mack for their invaluable insight, input, and discussions. The author would like to also thank Mariarosa Marinelli, Debopam Som, and Joel Green for their extensive review of this report.

References

Hilbert, B. (June 2012). *WFC3/IR Cycle 19 Bad Pixel Table Update*. Space Telescope WFC Instrument Science Report.

Hilbert, B. and P. R. McCullough (June 2009). *WFC3 SMOV Program 11420: IR Channel Functional Tests*. Space Telescope WFC Instrument Science Report.

Karson, Marvin (1968). "Handbook of Methods of Applied Statistics. Volume I: Techniques of Computation Descriptive Methods, and Statistical Inference. Volume II: Planning of Surveys and Experiments. I. M. Chakravarti, R. G. Laha, and J. Roy, New York, John Wiley; 1967". In: *Journal of the American Statistical Association* 63.323, pp. 1047–1049. DOI: 10.1080/01621459.1968.11009335. eprint: https://doi.org/10.1080/01621459.1968.11009335. URL: https://doi.org/10.1080/01621459.1968.11009335.

Sunnquist, B. (May 2019). *Generating Time-dependent WFC3/IR Bad Pixel Tables and Superdarks*. Space Telescope WFC3 Technical Instrument Report.

Sunnquist, B., G. Brammer, and S. Baggett (May 2019). *Time-dependent WFC3/IR Bad Pixel Tables*. Space Telescope WFC3 Instrument Science Report.